International Journal of Nanomedicine

Dovepress
open access to scientific and medical research

Open Access Full Text Article

ORIGINAL RESEARCH

Synthesis and Characterization of Graphene Oxide/Polyethylene Glycol/Folic Acid/Brucine Nanocomposites and Their Anticancer Activity on HepG2 Cells

Ibrahim Abdel Aziz Ibrahim[1], Abdullah R Alzahrani[1], Ibrahim M Alanazi[1], Naiyer Shahzad[1], Imran Shahid[1], Alaa Hisham Falemban[1], Mohd Fahami Nur Azlina[2], Palanisamy Arulselvan[3]

[1]Department of Pharmacology and Toxicology, Faculty of Medicine, Umm Al-Qura university, Makkah, Saudi Arabia; [2]Department of Pharmacology, Faculty of Medicine, Universiti Kebangsaan, Bangi, Selangor, Malaysia; [3]Department of Chemistry, Saveetha School of Engineering, Saveetha Institute of Medical and Technical Sciences (SIMATS), Saveetha University, Chennai, Tamil Nadu, 602 105, India

Correspondence: Ibrahim Abdel Aziz Ibrahim, Associated professor in Pharmacology, Department of Pharmacology and Toxicology, Faculty of Medicine, Umm Al-Qura University, Makkah, Saudi Arabia, Email iamustafa@uqu.edu.sa

Background: Liver cancer is the sixth most prevalent form of cancer and the second major cause of cancer-associated mortalities worldwide. Cancer nanotechnology has the ability to fundamentally alter cancer treatment, diagnosis, and detection.

Objective: In this study, we explained the development of graphene oxide/polyethylene glycol/folic acid/brucine nanocomposites (GO/PEG/Bru-FA NCs) and evaluated their antimicrobial and anticancer effect on the liver cancer HepG2 cells.

Methodology: The GO/PEG/Bru-FA NCs were prepared using the co-precipitation technique and characterized using various techniques. The cytotoxicity of the GO/PEG/Bru-FA NCs was tested against both liver cancer HepG2 and non-malignant Vero cells using an MTT assay. The antimicrobial activity of the GO/PEG/Bru-FA NCs was tested against several pathogens using the well diffusion technique. The effects of GO/PEG/Bru-FA NCs on endogenous ROS accumulation, apoptosis, and MMP levels were examined using corresponding fluorescent staining assays, respectively. The apoptotic protein expressions, such as Bax, Bcl-2, and caspases, were studied using the corresponding kits.

Results: The findings of various characterization assays revealed the development of GO/PEG/Bru-FA NCs with face-centered spherical morphology and an agglomerated appearance with an average size of 197.40 nm. The GO/PEG/Bru-FA NCs treatment remarkably inhibited the growth of the tested pathogens. The findings of the MTT assay evidenced that the GO/PEG/Bru-FA NCs effectively reduced the HepG2 cell growth while not showing toxicity to the Vero cells. The findings of the fluorescent assay proved that the GO/PEG/Bru-FA NCs increased ROS generation, reduced MMP levels, and promoted apoptosis in the HepG2 cells. The levels of Bax, caspase-9, and −3 were increased, and Bcl-2 was reduced in the GO/PEG/Bru-FA NCs-treated HepG2 cells.

Conclusion: The results of this work demonstrate that GO/PEG/Bru-FA NCs suppress viability and induce apoptosis in HepG2 cells, indicating their potential as an anticancer candidate.

Keywords: graphene oxide, brucine, nanomedicine, apoptosis, caspases, photoluminescence

Introduction

Hepatic cancer, often known as liver cancer, is the sixth most prevalent form of cancer overall and the second major cause of cancer-associated deaths worldwide.[1] By 2030, the World Health Organization (WHO) projects that over a million individual will die from liver cancer.[2,3] In addition, most cases of hepatic cancer are not diagnosed until they have developed to an advanced stage, when surgery becomes the primary treatment option for patients. Despite improvements in screening for early detection and treatment, the rates of liver cancer have increased along with its mortality.[4] The lifespan of cancer patients can be enhanced with conventional therapies, including radiotherapy, chemotherapy, and surgery. However, standard medical

Received: 17 October 2023
Accepted: 19 January 2024
Published: 5 February 2024

Graphical Abstract

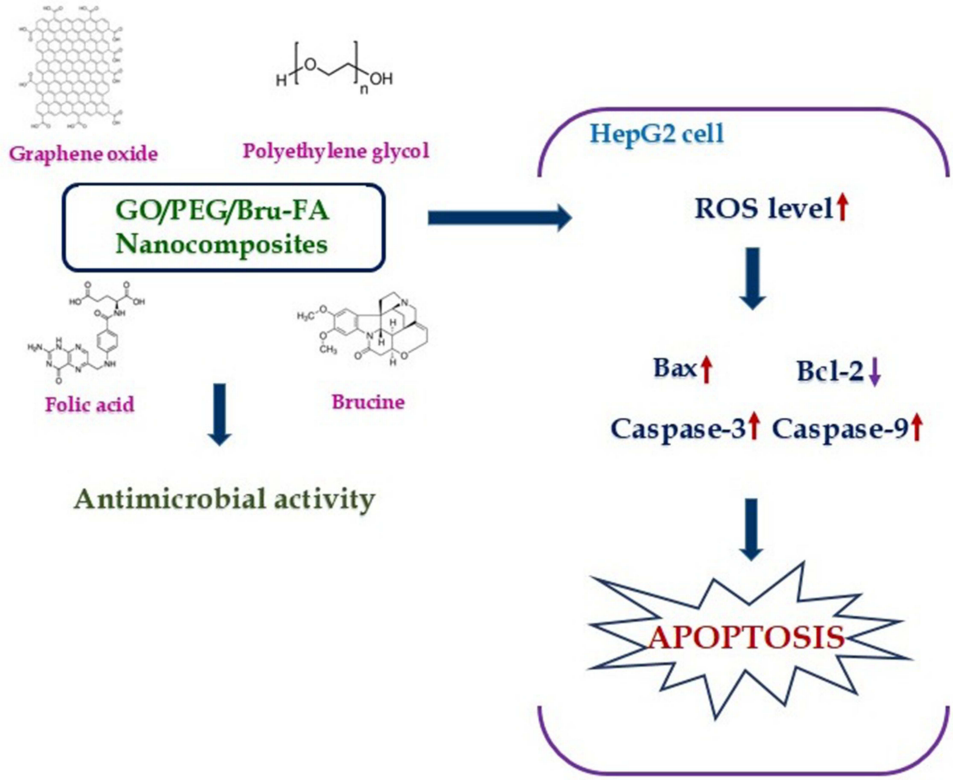

treatment options have side effects, which make cancer treatment difficult and must be managed.[5] Despite the fact that sorafenib is an FDA-approved drug for treating advanced liver cancer, low patient survival has still been observed with sorafenib. In addition, it has been proven that chemotherapy and radiotherapy are ineffective against hepatic cancer.[6] Hence, the finding of a novel, highly effective treatment for hepatic cancer is urgently required.

Nanomedicine has the potential to overcome the drawbacks of traditional drug delivery techniques such as poor oral bioavailability, low therapeutic indices, and nonspecific biodistribution.[7] Anticancer medicines and other therapeutic ligands can be delivered precisely and in controlled amounts by using nanocarriers derived from molecules with varying chemical compositions.[8] In cancer treatment, drug resistance is one of the biggest obstacles. Nanocarrier platforms that incorporate multiple chemotherapeutic drugs have been shown to be effective against tumor.[9] Meanwhile, most anticancer medicines have poor bioavailability because they are poorly soluble in water. Thus, the use of nanocarriers loaded with several medications has the potential to improve therapeutic efficacy while reducing adverse reactions and protecting against drug resistance. Chemotherapy drug resistance can be avoided, and the synergistic effect of many medications can be maximized when delivered by a nanocarrier.[10]

Due to their unique characteristics, nanomaterials can serve as nanocarriers in targeted drug delivery systems. For theranostic applications, the diagnostic and/or therapeutic substances can be coupled to nanomaterials.[11] Due to their distinctive physical and chemical characteristics, nanomaterials have recently found extensive usage in biomedicine, biotechnology, and other sectors, including the treatment of cancer.[12] Recently, nanomaterials have demonstrated a novel strategy for combating cancer, particularly liver cancer. Hepatocarcinoma has a high mortality rate and a poor prognosis for the long term. Hepatocarcinoma is expected to rise in prevalence over the next several decades.[13]

Graphene oxide (GO) is a hydrophilic nanocarrier with a high surface area, low cytotoxicity, biocompatibility, bioavailability, endocytosis activity, and mechanical properties.[14] GO is a promising nanocarrier for the nanodrug delivery system due to the

attachment of functional groups on its base and edge, allowing for the attachment and modification of different drugs.[15] The PEGylation procedure improved the GO's solubility in water. Polyethylene glycol (PEG)-conjugated GO improves the material's biocompatibility, allowing the anticancer medication to bind to the GO's surface.[16] PEG has been reported as a phase transition material and is a non-ionic, water-soluble polymer commonly utilized in drug delivery.[17] It has been highlighted that functionalizing GO with PEG increases its stability, and its biocompatibility makes it a suitable material for use in drug delivery.[18]

Brucine is a major bioactive compound found in the seeds of the Strychnos nux-vomica (Loganiaceae) plant. Numerous previous studies have already reported the pharmacological properties of brucine, including anti-tumor,[19] anti-inflammatory and analgesic,[20] and cardio-protective[21] activities. Recent studies have highlighted that brucine has anti-ulcer[22] and antidiabetic[23] effects. In this study, we explained the formulation of graphene oxide/polyethylene glycol/folic acid/brucine nanocomposites (GO/PEG/Bru-FA NCs). In addition, the characterization of the NCs, antimicrobial activity, in vitro cytotoxicity, and anticancer activity against liver cancer were explored.

Materials and Methods

Chemicals

Folic acid (59–30-3), brucine (357–57-3), PEG (25322–68-3), GO (796034), and other chemicals were purchased from Sigma-Aldrich, USA. To measure the biochemical indices, the assay kits were procured from Thermo Fisher Scientific, USA.

Preparation of GO/PEG/Bru-FA NCs

The GO/PEG/Bru-FA NCs were prepared by the co-precipitation technique. The 500 mg of synthetic GO and PEG were dissolved in 100 mL of deionized water. Then 100 mg of folic acid and 50 mg of brucine were added to the GO/PEG mixed solution. Then, 0.1 M NaOH was added very slowly while agitating the mixture at a temperature of about 60°C for 6 hours. The resultant nanopowder was washed with solutions of ethanol and distilled water until the necessary pH levels were reached. The resulting precipitate was dehydrated at 120°C for an hour, and the nanopowder was annealed in a 200°C oven for two hours to produce the GO/PEG/Bru-FA NCs.

Characterization of the Synthesized GO/PEG/Bru-FA NCs

UV-visible spectrum analysis was used to examine the formation of GO/PEG/Bru-FA NCs in the reaction suspension. Using a UV-visible spectrophotometer (Shimadzu-1700, Japan), we measured the development of GO/PEG/Bru-FA NCs and calculated their absorbance at various wavelengths between 400 and 1000 nm.

In order to study the crystalline nature of the synthesized GO/PEG/Bru-FA NCs, an X-ray diffractometer (X'pert Pro PANalytical System) was used to investigate the NCs at a wavelength range of λ=0.1541 nm with Cu-K radiation and the scan range set to 2=10-80°.

A SEM with EDAX spectroscopy was used to examine the prepared GO/PEG/Bru-FA NCs in order to investigate their morphology and elemental composition. With the help of a JEOL/EO JSM-5600 SEM analyzer (JEOL, Japan), the SEM and EDAX analyses were carried out.

The TEM (TECNAI F30, USA) was used to study the size and appearance of the synthesized GO/PEG/Bru-FA NCs. Briefly, the copper grid containing the synthesized GO/PEG/Bru-FA NCs was illuminated in a vacuum using electronic radiation. The electron beam was used to take microphotographs of the samples.

DLS analysis was carried out on the developed GO/PEG/Bru-FA NCs to measure their distribution patterns and particle size using the Zeta sizer (Malvern, USA) DLS equipment.

The stretching and bonding of synthesized GO/PEG/Bru-FA NCs were studied using FT-IR. Using a Shimadzu-8400S (Japan) spectrometer, we studied the GO/PEG/Bru-FA NCs to get a spectrum using the KBr disc at 4000–500 cm-1.

The photoluminescence spectra of the synthesized GO/PEG/Bru-FA NCs were measured using the spectrofluorimeter (Hitachi F-2500 FL Spectrophotometer).

Analysis of Antimicrobial Activity

The well diffusion method was employed to assess the antimicrobial efficacy of the synthesized GO/PEG/Bru-FA NCs against *Staphylococcus aureus, Streptococcus pneumonia, Klebsiella pneumonia, Escherichia coli, Bacillus megatarium, Pseudomonas aeruginosa*, and the fungi *Candida albicans*. The experiment used the respective agar growth medium. After inoculating the plates with corresponding pathogens, GO/PEG/Bru-FA NCs at concentrations of 1, 1.5, and 2 mg/mL were loaded into the wells, which are made using the cork borer on the surface of agar plates and incubated at 37°C for 24 hrs. After an incubation period, the diameter of the inhibitory zones was noted. Amoxicillin was utilized as a positive control in the experiments.

Cell Culture Collection

The liver cancer HepG2 and non-malignant Vero cells were procured from ATCC, USA, and grown on 10% FBS-enriched DMEM medium in a CO2 (5%) incubator. After the cells reached 80% confluency, they were trypsinized and employed for further assays.

MTT Assay

MTT assay was performed to examine the viability of GO/PEG/Bru-FA NCs-treated liver cancer HepG2 and non-malignant Vero cells. Both cells were grown separately in a 96-well plate for 24 hr before being treated with GO/PEG/Bru-FA NCs at several doses (2.5, 5, 7.5, 10, 15, and 20 µg/mL) for 24 hr at 37°C. Later, the MTT solution (20 µL) and DMEM (100 µL) for 4 hr. After the formed formazan deposits had been dissolved in DMSO (100 µL), the absorbance of the plate was taken at 570 nm.

Dual Staining

Apoptotic cell death in control and treated HepG2 cells was analyzed using a dual staining method. The HepG2 cells were grown in a 24-well plate for 24 hr before being exposed to 10 µg/mL of GO/PEG/Bru-FA NCs and/or 2 µg of DOX. Later, 100 µg/mL of AO/EB dyes were added to the wells and incubated in the dark for 5 min. Finally, the cells were analyzed under a fluorescence microscope to detect apoptosis in HepG2 cells.

DCFH-DA Staining

DCFH-DA fluorescent staining was used to examine the effect of GO/PEG/Bru-FA NCs on the generation of endogenous ROS in the HepG2 cells. The cells were grown in a 24-wellplate and subjected to GO/PEG/Bru-FA NCs (10 µg/mL) and 2 µg of DOX for 24 hr. After treatment, the cells were treated with 10 µL of DCFH-DA dye for 10 min, and the resulting fluorescence was measured using a fluorescent microscope.

DAPI Staining

The apoptotic cell nuclear morphology was examined by DAPI staining technique. Briefly, the HepG2 cells were loaded into a 24-well plate and then exposed to 10 µg/mL of GO/PEG/Bru-FA NCs and 2 µg of DOX for 24 hr. After treatment, cells were stained with DAPI (200 µg/mL) for 15 min after being fixed in paraformaldehyde (4%). The effects of GO/PEG/Bru-FA NCs on nuclear damage and apoptosis in HepG2 cells were subsequently investigated using a fluorescence microscope.

Rhodamine-123 (Rh-123) Staining

The MMP level in the treated HepG2 cells was analyzed by the Rh-123 staining method. The cells were exposed to 10 µg/mL of GO/PEG/Bru-FA NCs and/or 2 µg of DOX for 24 hr at 37°C. Then 10 µg/mL of Rh-123 dye was used to stain the cells for 3 min and finally, fluorescence microscopy was used to investigate the cells.

Analysis of Bax/Bcl-2 and Caspases Levels

Cell lysates from control and GO/PEG/Bru-FA NCs-exposed HepG2 cells were prepared and subjected to the analysis of expression of caspase-3, −9, Bax, and Bcl-2 using the corresponding ELISA assay kits using the manufacturer-recommended protocols (Thermofisher, USA).

Statistical Analysis

By using the GraphPad Prism software, the statistical analyses were done and the outcomes are represented as a mean ±SD of triplicate measurements. The significance level was measured using the one-way ANOVA and DMRT assays with $p<0.05$ as a significant.

Results

Characterization of the Synthesized GO/PEG/Bru-FA NCs

The presence of GO/PEG/Bru-FA NCs in the reaction solution was evidenced by UV-vis spectroscopic analysis, as shown in (Figure 1A). The absorbance was determined by measuring at a wavelength ranging from 400–1000 nm. Absorbance measurements show several characteristic peaks at 267 nm, 394 nm, 471 nm, 598 nm, 871 nm, and 1070 nm, which suggest the occurrence of the GO/PEG/Bru-FA NCs.

XRD analysis was done to study the crystallinity and purity of the produced GO/PEG/Bru-FA NCs, and the findings are revealed in (Figure 1B). The outcomes evidenced the occurrence of multiple peaks, which indicates that GO/PEG/Bru-FA NCs have a face-centered spherical structure with an average crystallographic size of 26.57 nm.

The elemental compositions of the formulated GO/PEG/Bru-FA NCs were studied with EDAX, and their morphology was evaluated using the SEM. SEM microphotographs (Figure 2A) showed that the formulated GO/PEG/Bru-FA NCs had a tetragonal and agglomerated appearance. The distinct peaks were observed in the elemental composition analysis by EDAX of the formulated GO/PEG/Bru-FA NCs, which correspond to carbon (C), nitrogen (N), and oxygen (O) (Figure 2B).

Figure 3 shows the findings of the TEM investigation of the synthesized GO/PEG/Bru-FA NCs, which characterized their shape, size, and distribution. The TEM micrographs showed that the developed GO/PEG/Bru-FA NCs were found in uneven shapes with a size of 45 nm. The crystallization of the GO/PEG/Bru-FA NCs was further validated by studying the SAED patterns.

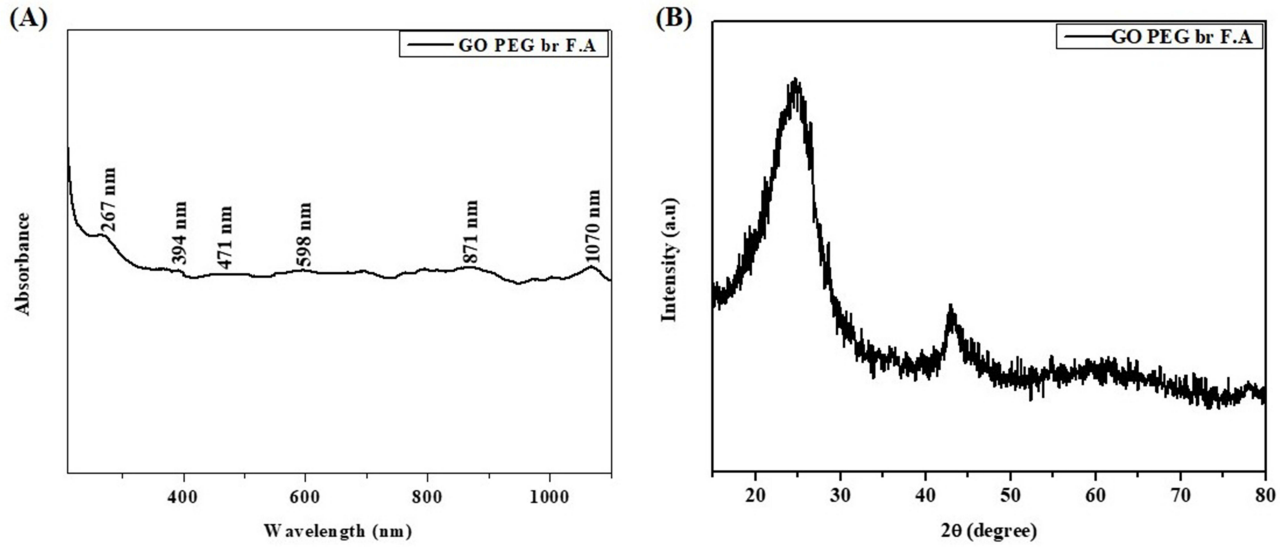

Figure 1 UV-visible spectroscopy and XRD analysis of the synthesized GO/PEG/Bru-FA NCs. Absorbance measurements show several characteristic peaks at 267 nm, 394 nm, 471 nm, 598 nm, 871 nm, and 1070 nm, which suggest the occurrence of the GO/PEG/Bru-FA NCs (**A**). The results proved the occurrence of multiple peaks, which indicates that GO/PEG/Bru-FA NCs have a face-centered spherical structure with an average crystallographic size of 26.57 nm (**B**).

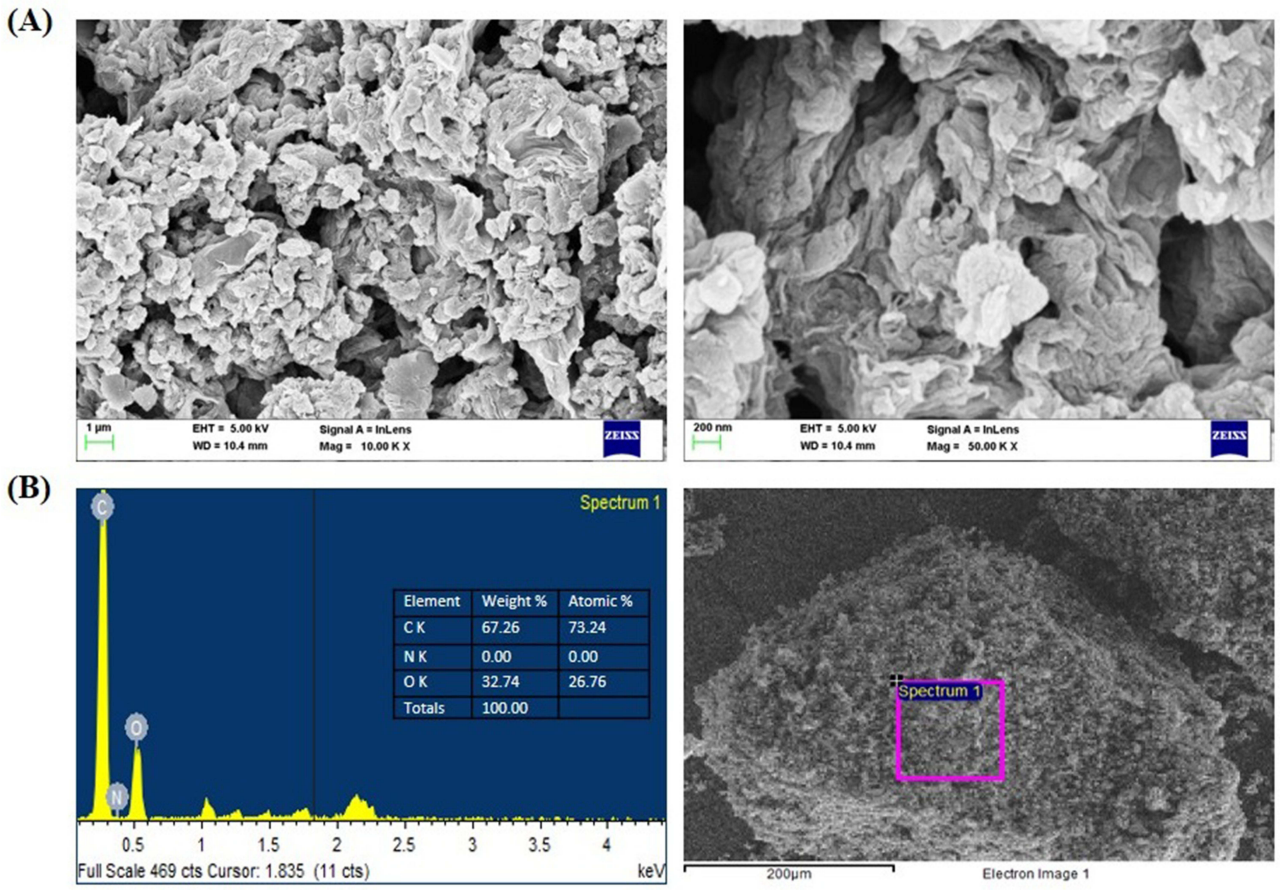

Figure 2 SEM and EDAX analysis of the synthesized GO/PEG/Bru-FA NCs. SEM images showed that the formulated GO/PEG/Bru-FA NCs had a tetragonal and agglomerated appearance (**A**). The distinct peaks were observed in the elemental composition analysis by EDAX, which correspond to carbon (C), nitrogen (N), and oxygen (O) (Figure 2B).

As seen in (Figure 4A and B), the results of the DLS analysis show the size and distribution patterns of the synthesized GO/PEG/Bru-FA NCs. The DLS results showed clear peaks, which confirmed the highly concentrated dispersion of the GO/PEG/Bru-FA NCs with an average size of 197.40 nm.

The results of FT-IR analysis, which determined the functional groups of the synthesized GO/PEG/Bru-FA NCs, are depicted in (Figure 5A). Many peaks at different frequencies were seen in the FT-IR spectrum of synthesized GO/PEG/Bru-FA NCs. O-H stretching causes the band to have strong peaks, like 3422 cm-1. The peaks at 2922 and 2853 cm-1 are characteristic of the stretching of hydroxyl groups. The 1702 cm-1 and 1563 cm-1 peaks, as well as the 1375 cm-1 and 1044 cm-1, are indicative of the C-H, C-O, and H-O bending vibrations, respectively.

The synthesized GO/PEG/Bru-FA NCs were subjected to PL spectroscopic to study. The PL spectra of the GO/PEG/Bru-FA NCs revealed characteristic peaks at 376.79, 396.92, 403.61, 412.70, 423.58, 445.96, 481.77, and 521.32 (Figure 5B). The UV emission at 376.79 and 396.92 nm was triggered by a O2 vacancies (VO°). When VO++ is close to VB, leading to violet emission at 403.61 and 412.70 nm. The blue emission at 423.58 nm, 445.96 nm, and 481.77 nm is caused by two different processes: the transition from the donor level to the valence band induced by (VO+) and the transition of electrons from O2 vacancies VO° to doubly ionized O2 vacancies (VO++). Green fluorescence at 521.32 nm was attributed to oxygen vacancies.

Antimicrobial Effects of the GO/PEG/Bru-FA NCs

The antimicrobial efficacy of the GO/PEG/Bru-FA NCs against pathogens including *S. pneumoniae, S. aureus, E. coli, K. pneumoniae, B. megatarium*, and *P. aeruginosa* and the fungi *C. albicans* was assessed using the well diffusion

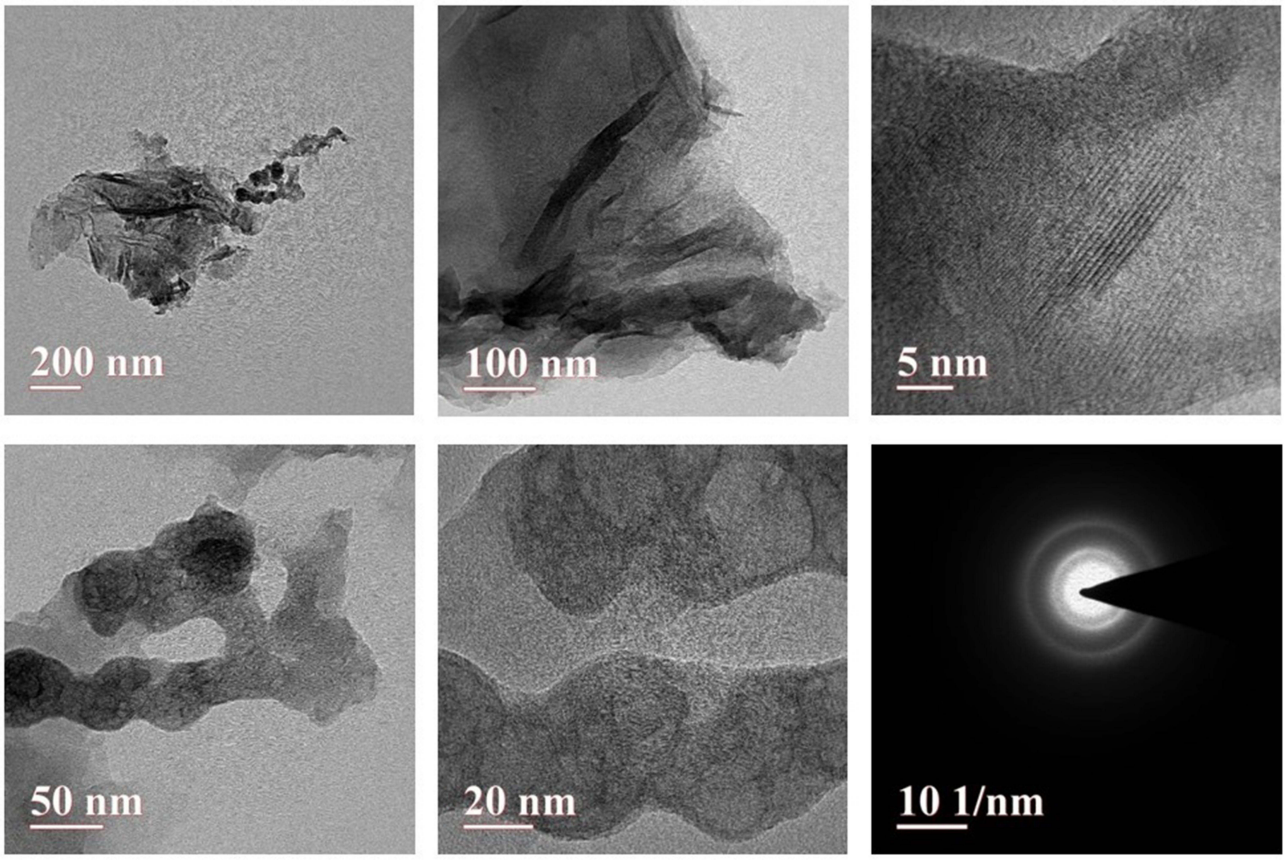

Figure 3 TEM analysis of the synthesized GO/PEG/Bru-FA NCs. The TEM images revealed that the developed GO/PEG/Bru-FA NCs were found in uneven shapes with an average size of 45 nm. The crystallization of the GO/PEG/Bru-FA NCs was further validated by the SAED patterns.

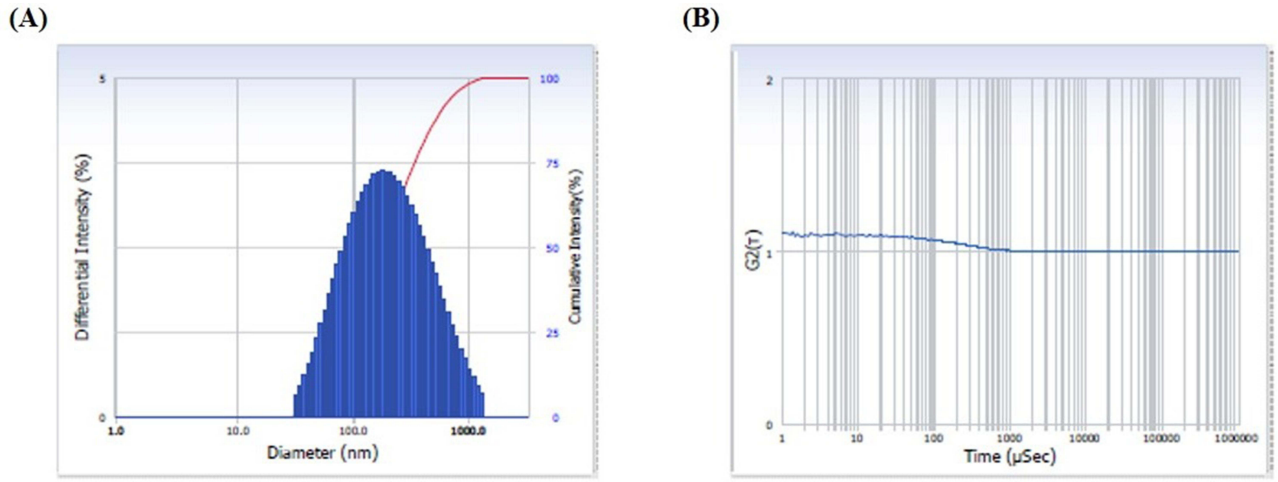

Figure 4 DLS analysis of the synthesized GO/PEG/Bru-FA NCs. The DLS results showed clear peaks, which confirmed the highly concentrated dispersion of the GO/PEG/Bru-FA NCs with an average size of 197.40 nm. (**A**): DLS graph of the light intensity with estimated particle size. (**B**): Autocorrelation function.

technique, as shown in Figure 6. The treatment with the different doses of the synthesized GO/PEG/Bru-FA NCs revealed excellent antimicrobial properties against all the tested pathogens, which resembles the results of the amoxicillin results. GO/PEG/Bru-FA NCs inhibited the growth of these pathogens, especially *S. aureus* (25 mm), *K. pneumoniae*

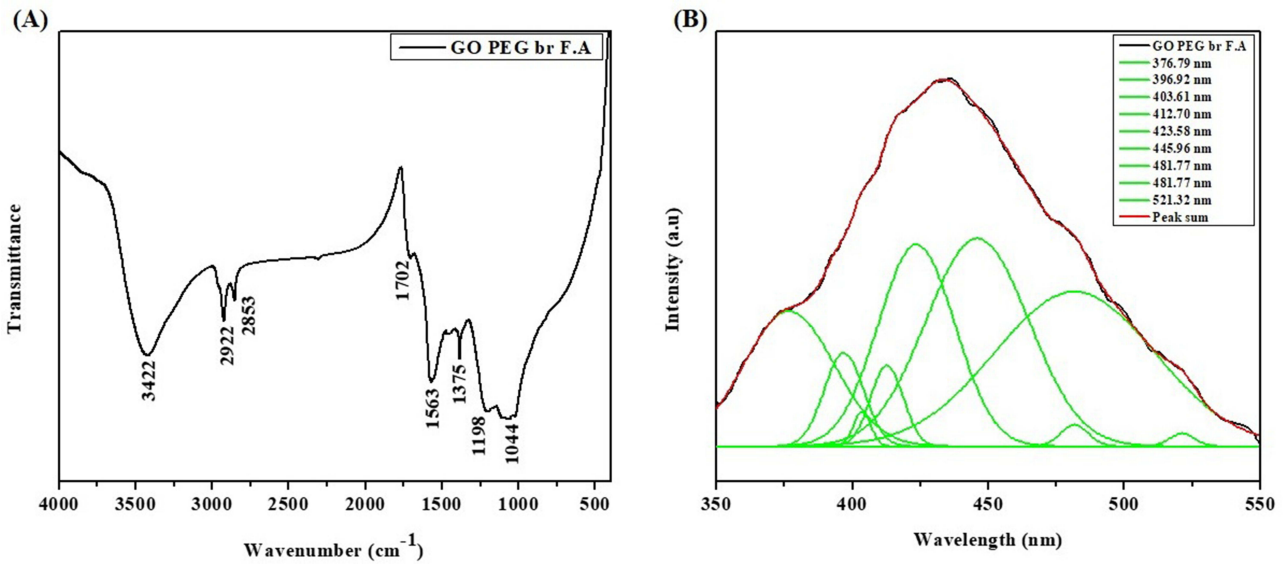

Figure 5 FT-IR and Photoluminescence spectral analysis of the synthesized GO/PEG/Bru-FA NCs. (**A**): Several at different frequencies were seen in the FT-IR spectrum of synthesized GO/PEG/Bru-FA NCs, which corresponds to the various stretching and bonding. (**B**): The PL spectra of the GO/PEG/Bru-FA NCs reveal characteristic peaks due to the O2 vacancies (VO°), the transition from the donor level to the valence band induced by VO+, and the transition of electrons from O2 vacancies (VO°) to doubly ionized O2 vacancies (VO++), and oxygen vacancies.

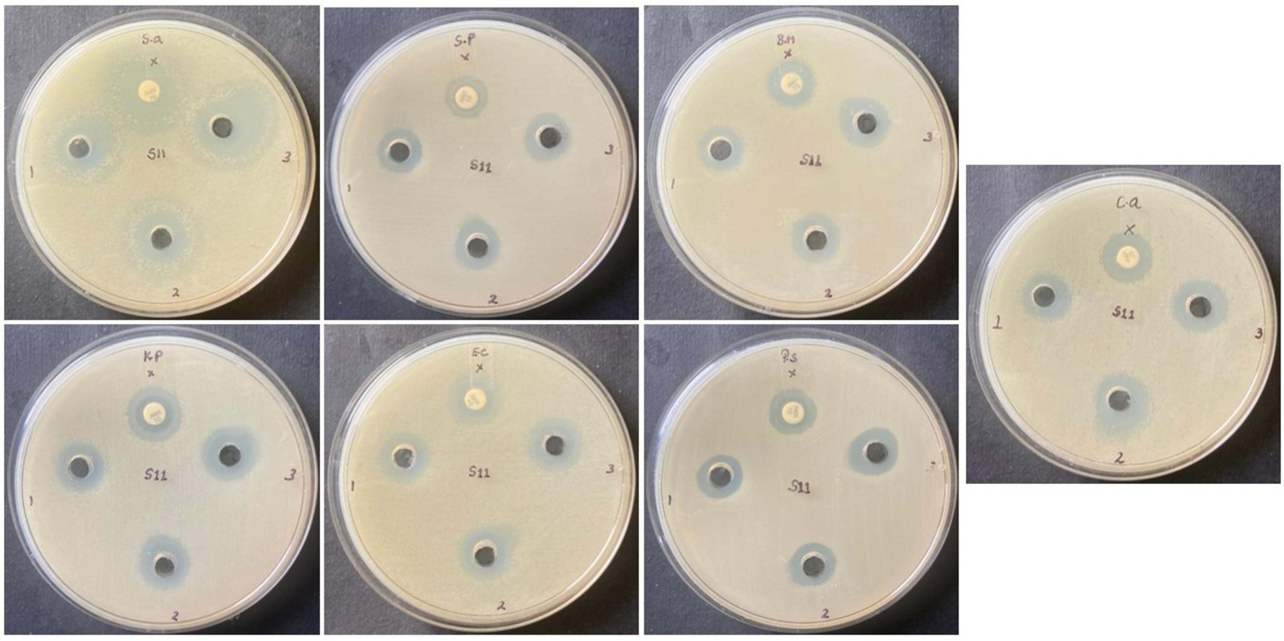

Figure 6 Antimicrobial activity of the synthesized GO/PEG/Bru-FA NCs. The results proved that the GO/PEG/Bru-FA NCs treatment substantially inhibited the growth of the tested pathogens. Particularly, *(S)aureus, (K) pneumoniae, (E)coli*, and *C. albicans* showed maximum sensitivity to the GO/PEG/Bru-FA NCs treatment.

(16 mm), *E. coli* (17 mm), and *C. albicans* (17 mm) showed maximum sensitivity against the GO/PEG/Bru-FA NCs (Figure 7).

Effect of GO/PEG/Bru-FA NCs on the Viability of HepG2 and Vero Cell Lines

The findings of an MTT cytotoxicity assay showing the effect of GO/PEG/Bru-FA NCs on the growth of HepG2 and Vero cells are demonstrated in Figure 8. The GO/PEG/Bru-FA NCs at diverse doses (2.5–20 µg/mL) significantly ($p<0.05$) reduced HepG2 cell viability. However, the GO/PEG/Bru-FA NCs treatment at the same concentrations (2.5–20 µg/mL) had no considerable

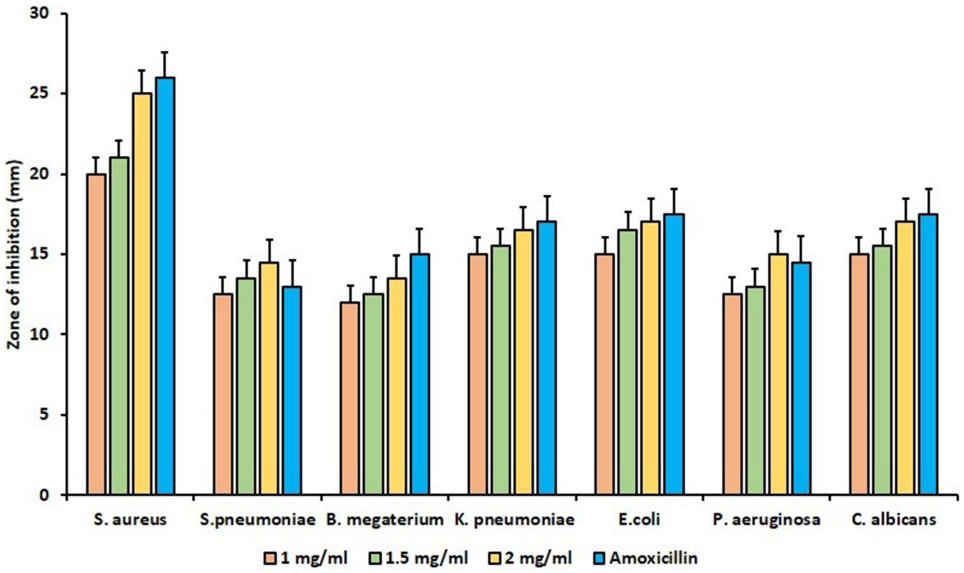

Figure 7 Antimicrobial activity of the synthesized GO/PEG/Bru-FA NCs. The values are presented as a mean±SD of triplicate measurements. The data are statistically studied by one-way ANOVA and DMRT assays using the GraphPad Prism software.

effect on the growth of nonmalignant Vero cells. The GO/PEG/Bru-FA NCs were found to have an IC50 of 10 µg/mL against HepG2 liver cancer cells; hence, this concentration was chosen for further study.

Effect of GO/PEG/Bru-FA NCs on the ROS Accumulation in the HepG2 Cells

The findings of an analysis of the effects of GO/PEG/Bru-FA NCs treatment on endogenous ROS generation in HepG2 cells are shown in Figure 9. Green fluorescence was significantly enhanced in HepG2 cells after treatment with 10 µg/mL of GO/PEG/Bru-FA NCs compared to control. These increases in green fluorescence are due to the increase in endogenous ROS generation in the GO/PEG/Bru-FA NCs-exposed HepG2 cells. The increase in green fluorescence after treatment with the standard drug DOX is further evidence that GO/PEG/Bru-FA NCs have promoted endogenous ROS accumulation in the HepG2 cells.

Effect of GO/PEG/Bru-FA NCs on the Apoptosis in the HepG2 Cells

Figure 10A displays the results of dual staining performed to evaluate the apoptosis in both control and GO/PEG/Bru-FA NCs-exposed HepG2 cells. Treatment of HepG2 cells with 10 µg/mL of GO/PEG/Bru-FA NCs resulted in increased yellow and orange fluorescence, demonstrating the occurrence of both early and late apoptotic cell deaths, respectively. More cells with strong yellow/orange fluorescence were also observed after DOX treatment, supporting the apoptosis inducing potentials of the GO/PEG/Bru-FA NCs.

Effect of GO/PEG/Bru-FA NCs on the MMP Level in the HepG2 Cells

Rh-123 staining assay results of GO/PEG/Bru-FA NCs-treated HepG2 cells are shown in (Figure 10B). Green fluorescence was abundant in control cells, demonstrating an intact and normal MMP level. However, treatment of the HepG2 cells with 10 µg/mL of GO/PEG/Bru-FA NCs resulted in a reduction in MMP level, as demonstrated by a reduction in green fluorescence. The results of the DOX treatment also showed a reduction in MMP level, which supports the activity of GO/PEG/Bru-FA NCs.

Effect of GO/PEG/Bru-FA NCs on the Apoptosis in the HepG2 Cells

Figure 10C reveals the findings of a DAPI staining analysis in both control and GO/PEG/Bru-FA NCs-treated HepG2 cells. The more apoptotic incidences, including chromatin condensation, nuclear damage, membrane rupture, apoptotic body developments, and loss in cell numbers, were observed in the HepG2 cells after treatment with 10 µg/mL of GO/

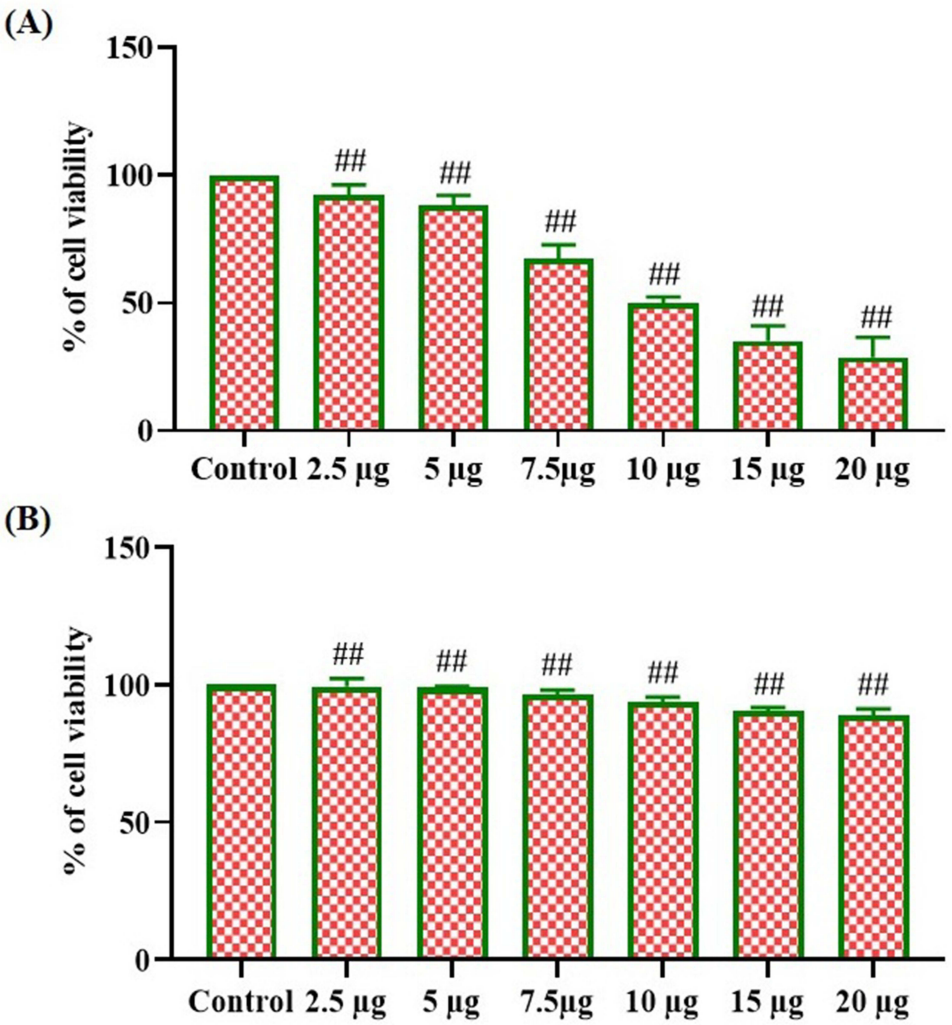

Figure 8 Effect of GO/PEG/Bru-FA NCs on the viability of HepG2 and Vero cell lines. The values are presented as a mean±SD of triplicate measurements. The data are statistically studied by one-way ANOVA and DMRT assays using the GraphPad Prism software.
Notes: ##Represents that the values are significantly differ from control at $p<0.05$. (**A**): Liver cancer HepG2 cells; (**B**): Non-malignant Vero cells.

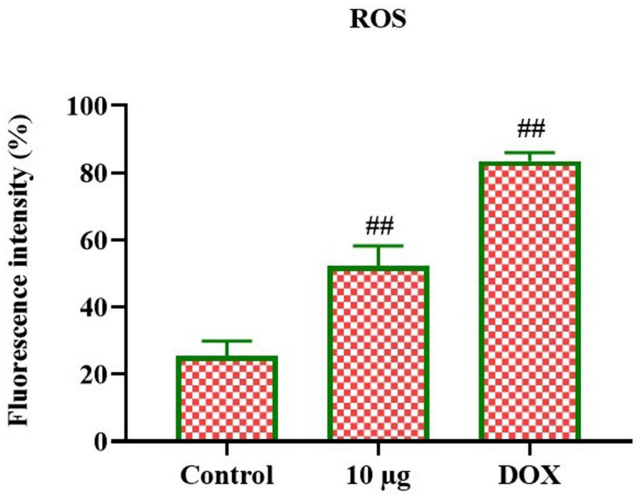

Figure 9 Effect of GO/PEG/Bru-FA NCs on the ROS generation in the HepG2 cells. The values are given as a mean±SD of triplicate measurements. The data are statistically studied by one-way ANOVA and DMRT assays using the GraphPad Prism software.
Note: ##Represents that the values are significantly differ from control at $p<0.05$.

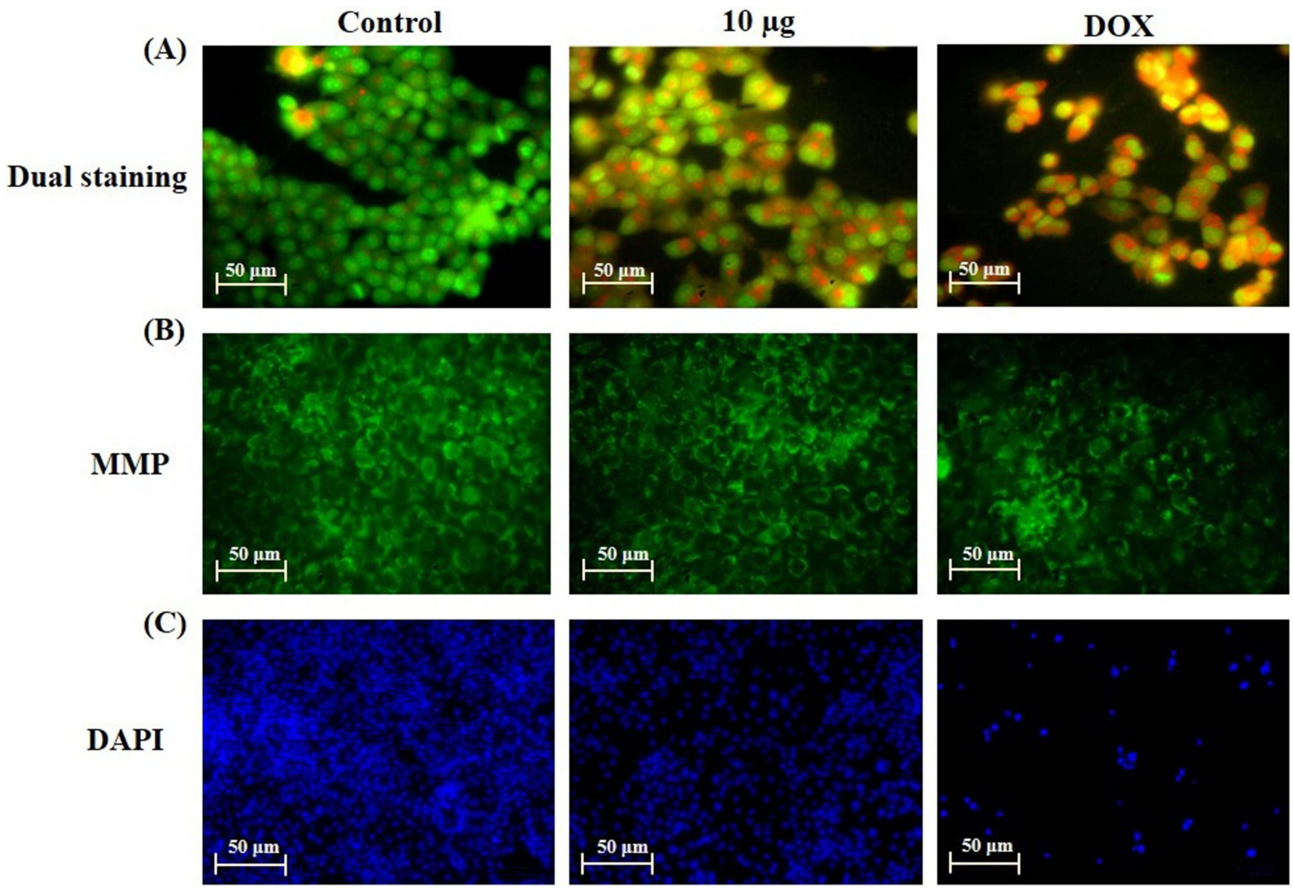

Figure 10 Effect of GO/PEG/Bru-FA NCs on the apoptosis and MMP level in the HepG2 cells. The HepG2 cells revealed an increased yellow and Orange fluorescence after treatment with 10 µg/mL of GO/PEG/Bru-FA NCs or 2 µg of standard drug DOX, which indicates the occurrence of apoptosis (**A**). The GO/PEG/Bru-FA NCs treatment (10 µg/mL) causes a considerable decrease in the MMP level of HepG2 cells. The control cells revealed more green fluorescent cells, which indicates normal and intact MMP (**B**). The 10 µg/mL of GO/PEG/Bru-FA NCs treatment revealed a higher incidences of cell and nuclear damages, loss in cell numbers, and appearance of apoptotic bodies, which showed that the GO/PEG/Bru-FA NCs treatment promoted apoptosis in the HepG2 cells. The fluorescent microscope was utilized to detect the intensity of the fluorescence (**C**). Scale bar: 50 µm.

PEG/Bru-FA NCs. Similar apoptotic incidences were also noted in the DOX-treated HepG2 cells, which proves the apoptotic-inducing potentials of the formulated GO/PEG/Bru-FA NCs on the liver cancer cells.

Effect of GO/PEG/Bru-FA NCs on the Apoptotic Protein Expressions in the HepG2 Cells

Apoptotic protein expressions, including bax, Bcl-2, caspase-9, and −3, in control and GO/PEG/Bru-FA NCs-treated HepG2 liver cancer cells were analyzed, and the outcomes are revealed in Figure 11. In contrast to the control cells, the GO/PEG/Bru-FA NCs-treated HepG2 cells had reduced levels of Bcl-2 and increased levels of Bax, caspase-9, and −3. The findings of DOX treatment corroborated these observations by elevating apoptotic protein expression in HepG2 cells. As a result, it was clear that the GO/PEG/Bru-FA NCs treatment has induced apoptosis (cell death) in HepG2 liver cancer cells.

Discussion

Liver cancer is the foremost cause of cancer-associated mortality worldwide, and its prevalence is rapidly increasing every year. Furthermore, it is challenging to diagnose liver cancer in the early stages, and the prognosis is not satisfactory.[24] In addition, liver cancer is highly metastatic to the lungs and bones, which makes local therapy less effective.[25] In addition, the prognosis for individuals with liver cancer is particularly poor due to its insensitivity to treatment and high metastatic potential.[26] Cancer

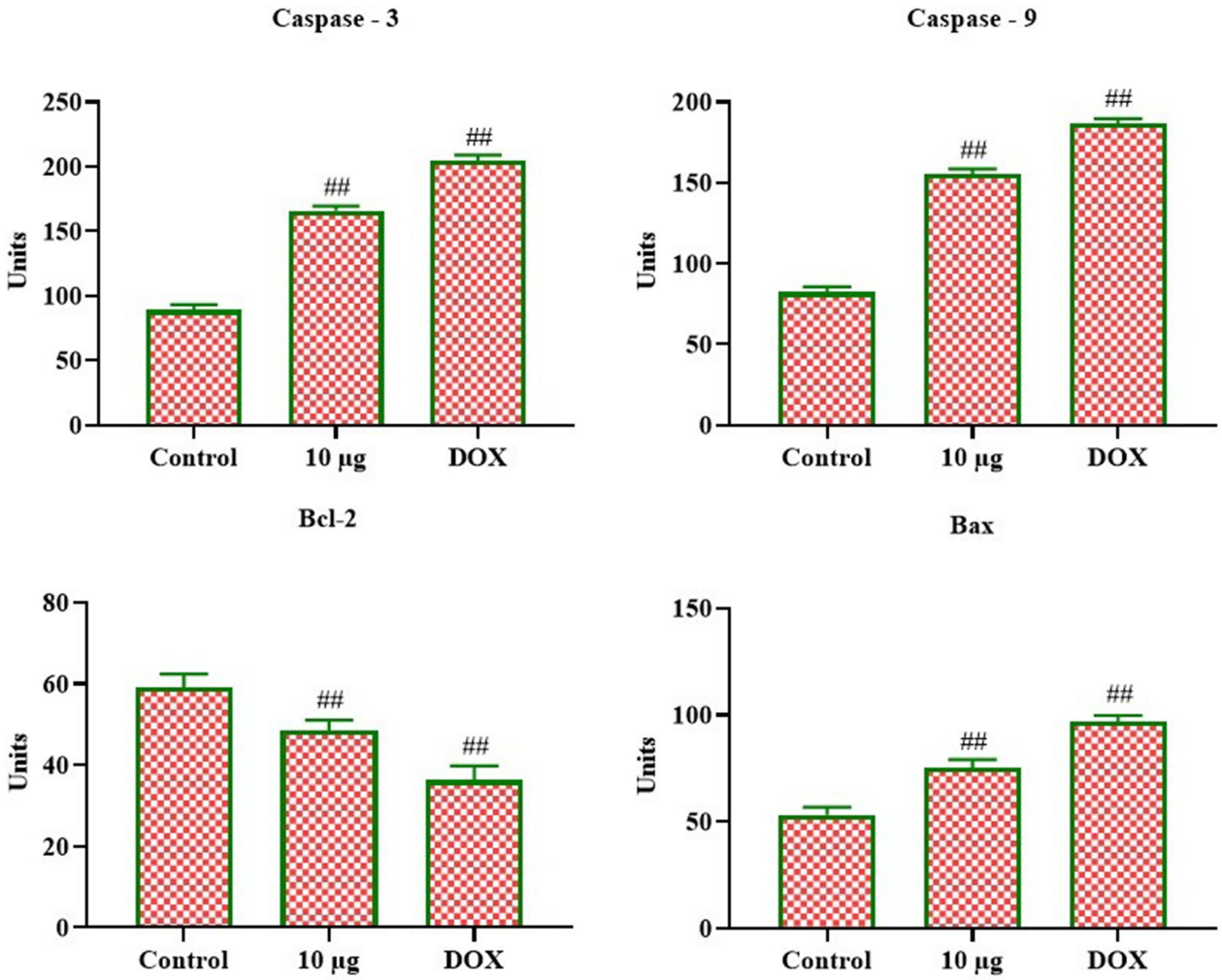

Figure 11 Effect of GO/PEG/Bru-FA NCs on the apoptotic protein expressions in the HepG2 cells. The values are given as a mean±SD of triplicate measurements. The data are statistically studied by one-way ANOVA and DMRT assays using the GraphPad Prism software.
Note: ##Represents that the values are significantly differ from control at $p<0.05$.

nanotechnology has the ability to fundamentally alter cancer treatment, diagnosis, and detection.[27] Nano-biotechnology applications have recently shown new strategies for cancer diagnosis and treatment.[28]

The early detection, diagnosis, and effective delivery of anticancer medications made possible by nanotechnology has been shown to reduce the likelihood of toxic side effects and increase patient survival.[29] One of the endeavors in nanomedicine for cancer therapy is the use of a dual medication nanodelivery system. To improve antitumor activity against cancer cells, researchers have explored the use of dual drug nanodelivery, in which two or more chemotherapeutic drug combinations are delivered together via a nanocarrier delivery system.[30] Due to its central role in the reduction of drug-related adverse effects, the enhancement of therapeutic efficacy, and the extension of bioavailability, drug delivery is the focus of intense research and development in the field of nanomedicine.[31,32] Therefore, here we formulated the GO/PEG/Bru-FA NCs and examined their anticancer effects against liver cancer cells.

Prior to their application in medicine, characterizing the GO/PEG/Bru-FA NCs is essential to understanding their characteristics.[33,34] Characterizing the GO/PEG/Bru-FA NCs is a step toward understanding their functionality and developing methods for their controlled production for therapeutic applications.[35,36] The newly produced GO/PEG/Bru-FA NCs were confirmed using UV-vis spectral analysis. The crystalline nature of the newly synthesized GO/PEG/Bru-FA NCs was further confirmed by XRD analysis. The SEM image revealed more information on the shape and appearance of the GO/PEG/Bru-FA NCs, which have a tetragonal and agglomerated appearance. The size and morphology of the GO/PEG/Bru-FA NCs were

examined with TEM. The TEM findings clearly demonstrate that the freshly generated GO/PEG/Bru-FA NCs were of uneven shapes, and the DLS study findings revealed an average particle size of 197.40 nm.[37–39]

By passively targeting the tumor, NCs loaded with anticancer medications can increase the permeability and retention impact, extending the drug circulation time in the blood.[40] However, ligand-based active targeting is aided by membrane-receptor upregulation in cancer cells. Improved anticancer efficacy has been observed in clinical trials, including the multidrug delivery of passive and active targeted therapy.[41] Common chemotherapies are not selective for tumor cells and often cause harmful side effects in normal cells. The toxic effects of chemotherapy can be mitigated by administering the medicine directly into the tumor cell and targeting it at the tumor site. NCs can be used for passive targeting, which makes use of the tumor's specific pathophysiological properties to direct the release of therapeutic medicines at the tumor site.[42] The cytotoxicity assay is one of the most useful tools in toxicology because it can reveal details on cell growth, death, and metabolic activities in response to harmful substances.[43] This study used the MTT assay to test the cytotoxic effects of GO/PEG/Bru-FA NCs at various concentrations for their ability to inhibit cell growth against both liver cancer HepG2 and non-malignant Vero cells. The findings proved that the GO/PEG/Bru-FA NCs treatment considerably reduced the viability of HepG2 cells while not showing toxicity to normal Vero cells.

Toxic effects from nanomaterials on tumor cells can be caused, in part, by the increased generation of ROS and oxidative stress. Though ROS are produced in biological systems as a regular part of metabolic activities, it is well established that ROS generation plays a key role in the mechanism of cell proliferation and differentiation. It is well known that the excess production of ROS is connected with the activation of cell apoptosis, and the overproduction of ROS has been linked in particular to anticancer treatments.[44] When ROS are produced in greater quantities than their removal by antioxidants, it results in oxidative stress. Increased ROS generation and oxidative stress cause DNA damage and apoptosis.[45] Nanoscale materials have a high surface area-to-volume ratio, which increases their chemical reactivity and, in turn, their ability to generate intracellular ROS. In this study, our findings also proved that the GO/PEG/Bru-FA NCs enhanced the generation of endogenous ROS production in the liver cancer HepG2 cells. Hence, it was clear that the GO/PEG/Bru-FA NCs treatment can facilitate oxidative stress-mediated cell death in the liver cancer cells.

Apoptosis is a cell death mechanism that helps prevent tumor progression by eliminating cells that have been genetically altered or are premalignant. Since blocking apoptosis in mutant cells could cause them to transform into cancerous cells, this process is often considered a mainstay of an effective anti-cancer therapy. Failure of apoptosis can result in uncontrolled cell growth and, ultimately, tumor formation.[46] In this study, the hallmarks of apoptosis, such as chromatin condensation, nuclear fragmentation, and DNA integrity, were seen in the HepG2 cells after treatment with the GO/PEG/Bru-FA NCs, which are assessed using dual staining, indicating the presence of apoptosis.[47,48]

DNA fragmentation and membrane rupturing are hallmarks of apoptosis, and both contribute to an increase in the permeability of the cell membrane. The DAPI fluorescent stain is able to enter the nucleus and bind to the DNA fragments in apoptotic cells better than in nonapoptotic cells because of the larger pores in the nuclear membranes of apoptotic cells. Bright fluorescent patches, known as apoptotic bodies, can be seen inside these cells as a result of this process.[49] Therefore, apoptotic cell nuclear morphology in GO/PEG/Bru-FA NCs-exposed HepG2 cells was analyzed using DAPI staining. The study found that the GO/PEG/Bru-FA NCs-treated HepG2 cells appeared to have undergone apoptosis, cellular damage, and cell volume loss.

The onset or inhibition of apoptosis heavily depends on the balance between pro- and anti-apoptotic protein expressions. Cancer cells commonly overexpress anti-apoptotic genes to aid in survival, growth, and resistance to therapy. Thus, cancer is characterized by a breakdown in apoptotic processes.[50] The Bcl-2 family, which includes both Bcl-2 and Bax, is essential for regulating apoptosis. Apoptosis, the controlled cell death mechanism, is an essential biological process that is controlled by the Bcl-2 family of proteins. Bax, which promotes apoptosis, and Bcl-2, which reduces apoptosis, are two pro- and anti-apoptotic proteins, respectively, that regulate cell death. In order to evade cell death and continue dividing, cancer cells frequently overexpress Bcl-2. Apoptosis resistance can be caused, in part, by decreased Bax expression and increased Bcl-2 expression in cancer cells.[51] Increased levels of Bcl-2 have been associated with carcinogenesis, tumor angiogenesis, and other malignant outcomes. Anticancer medications primarily induce cell death in tumor cells through the process of apoptosis. Targeting the Bcl-2 protein may improve the efficacy of chemotherapeutics that induce apoptosis.[52] The inactivation of caspases enhances cancer development and apoptosis resistance in tumor cells.[53] Disrupting Bcl-2 and Bax can lead to a reduction in caspase-3 activity, which in turn can help tumor cells avoid apoptosis. In this work, our findings proved that the GO/PEG/Bru-FA NCs treatment

considerably reduced Bcl-2 expression while promoting Bax, caspase-9, and −3 expressions in the liver cancer HepG2 cells. Therefore, it was clear that the GO/PEG/Bru-FA NCs promote apoptotic protein expression and facilitate apoptosis in the liver cancer cells.

Although the successful formulation of GO/PEG/Bru-FA NCs as anticancer candidates has been achieved, there are still certain limits to consider, such as the possibility of the long-term toxicity of these NCs. The present work consists of only brief in vitro experiments that fail to sufficiently represent the prolonged safety of NCs. Hence, prior to the unrestricted use of these NCs in clinical settings, further research will be required, including examinations of the NC's in vivo characteristics, particularly their impact on the biological system.

Conclusion

The results of the present work demonstrate that GO/PEG/Bru-FA NCs suppress cell growth and induce apoptosis in HepG2 cells, indicating their potential as an anticancer candidate. Apoptosis was induced in HepG2 cells after treatment with GO/PEG/Bru-FA NCs, which promoted the expression of pro-apoptotic proteins. Therefore, GO/PEG/Bru-FA NCs have the capacity to be an effective anticancer candidate in the treatment of liver cancer. In addition, more studies are still needed to determine the molecular pathways involved in GO/PEG/Bru-FA NCs-induced apoptosis in liver cancer cells so that they can be developed for liver cancer treatment in the future.

Data Available Statement

Available upon request from the corresponding author.

Acknowledgment

The authors extend their appreciation to the Deanship for Research & Innovation, Ministry of Education in Saudi Arabia for funding this research work through the project number: IFP22UQU4331277DSR123.

Author Contributions

All authors made a significant contribution to the work reported, whether that is in the conception, study design, execution, acquisition of data, analysis and interpretation, or in all these areas; took part in drafting, revising or critically reviewing the article; gave final approval of the version to be published; have agreed on the journal to which the article has been submitted; and agree to be accountable for all aspects of the work.

Disclosure

The authors report no conflicts of interest in this work.

References

1. Ogunwobi OO, Harricharran T, Huaman J, et al. Mechanisms of hepatocellular carcinoma progression. *World J Gastroenterol*. 2019;25(19):2279–2293. doi:10.3748/wjg.v25.i19.2279
2. Villanueva A, Longo DL. Hepatocellular carcinoma. *N Engl J Med*. 2019;380(15):1450–1462. doi:10.1056/NEJMra1713263
3. Siegel RL, Miller KD, Jemal A. Cancer statistics, 2019. *CA Cancer J Clin*. 2019;69(1):7–34. doi:10.3322/caac.21551
4. Balogh J, Victor D, Emad HA. Hepatocellular carcinoma: a review. *J Hepatocell Carcinoma*. 2016;3:41–53. doi:10.2147/JHC.S61146
5. Rao PV, Nallappan D, Madhavi K, Rahman S, Jun Wei L, Gan SH. Phytochemicals and biogenic metallic nanoparticles as anticancer agents. *Oxid Med Cell Longev*. 2016;33:12–27.
6. Daher S, Massarwa M, Benson AA, Khoury T. Current and future treatment of hepatocellular carcinoma: an updated comprehensive review. *J Clin Transl Hepatol*. 2018;6(1):69–78. doi:10.14218/JCTH.2017.00031
7. Yesildag C, Tyushina A, Lensen M, Yesildag C. Nano-contact transfer with gold nanoparticles on PEG hydrogels and using wrinkled PDMS-stamps. *Polymers*. 2017;9(6):199. doi:10.3390/polym9060199
8. Qiu L, Chen T, Öçsoy I, et al. A cell-targeted, size-photocontrollable, nuclear-uptake nanodrug delivery system for drug-resistant cancer therapy. *Nano Lett*. 2015;15(1):457–463. doi:10.1021/nl503777s
9. Navya PN, Kaphle A, Srinivas SP, Bhargava SK, Rotello VM, Daima HK. Current trends and challenges in cancer management and therapy using designer nanomaterials. *Nano Converg*. 2019;6:23.
10. Gurunathan S, Kang MH, Qasim M, Kim JH. Nanoparticle-mediated combination therapy: two-in-one approach for cancer. *Int J Mol Sci*. 2018;19(10):3264. doi:10.3390/ijms19103264

11. Baig B, Halim SA, Farrukh A, Greish Y, Amin A. Current status of nanomaterial-based treatment for hepatocellular carcinoma. *Biomed Pharmacother*. 2019;116:108852.
12. Fiorillo M, Verre AF, Iliut M, et al. Graphene oxide selectively targets cancer stem cells, across multiple tumor types: implications for non-toxic cancer treatment, via "differentiation-based nano-therapy". *Oncotarget*. 2015;6(6):3553–3562. doi:10.18632/oncotarget.3348
13. Siegel RL, Miller KD, Jemal A. Cancer statistics. *CA Cancer J Clin*. 2016;66(1):7–30. doi:10.3322/caac.21332
14. Colone M, Calcabrini A, Stringaro A. Drug delivery systems of natural products in oncology. *Molecules*. 2020;25:4560. doi:10.3390/molecules25194560
15. Buskaran K, Hussein MZ, Mohd-Moklas MA, Fakurazi S. Morphological changes and cellular uptake of functionalized graphene oxide loaded with protocatechuic acid and folic acid in hepatocellular carcinoma cancer cell. *Int J Mol Sci*. 2020;21(16):5874. doi:10.3390/ijms21165874
16. Valcarcel M, Roura-Ferrer M. Promising antioxidant and anticancer (Human Breast Cancer) oxidovanadium(IV) complex of chlorogenic acid. synthesis, characterization and spectroscopic examination on the transport mechanism with bovine serum albumin. *J Inorg Biochem*. 2014;135:86–99. doi:10.1016/j.jinorgbio.2014.02.013
17. Fu Y, Xiong W, Wang J, Li J, Mei T, Wang X. Polyethylene glycol based graphene aerogel confined phase change materials with high thermal stability. *J Nanosci Nanotechnol*. 2018;18(5):3341–3347. doi:10.1166/jnn.2018.14635
18. Siritham C, Thammakhet-Buranachai C, Thavarungkul P, Kanatharana P. A stir foam composed of graphene oxide, poly(ethylene glycol) and natural latex for the extraction of preservatives and antioxidant. *Mikrochim Acta*. 2018;185:148.
19. Qin JM, Yin PH, Li Q, et al. Anti-tumor effects of brucine immuno-nanoparticles on hepatocellular carcinoma. *Int J Nanomed*. 2012;7(1):369–379. doi:10.2147/IJN.S27226
20. Yin W, Wang TS, Yin F, Cai BC. Analgesic and anti-inflammatory properties of brucine and brucine N-oxide extracted from seeds of Strychnos nux-vomica. *J Ethnopharmacol*. 2003;88(3):205–214. doi:10.1016/S0378-8741(03)00224-1
21. Liu B, Zhang Y, Wu Q, Wang L, Hu B. Alleviation of isoprenaline hydrochloride induced myocardial ischemia injury by brucine through the inhibition of Na+/K+-ATPase. *Exp Gerontol*. 2021;149(1):111332. doi:10.1016/j.exger.2021.111332
22. Noman M, Qazi NG, Rehman NU, Khan AU. Pharmacological investigation of brucine anti-ulcer potential. *Front Pharmacol*. 2022;13:886433. doi:10.3389/fphar.2022.886433
23. Khan NU, Qazi NG, Khan AU, Ali F, Hassan SSU, Bungau S. Anti-diabetic activity of brucine in streptozotocin-induced rats: in silico, in vitro, and in vivo studies. *ACS Omega*. 2022;7(50):46358–46370. doi:10.1021/acsomega.2c04977
24. Zhu B, Li YH, Lin ZF, et al. Silver nanoparticles induce HePG-2 cells apoptosis through ROS-mediated signaling pathways. *Nanoscale Res Lett*. 2016;11(1):98–205. doi:10.1186/s11671-016-1419-4
25. Thapa RK, Choi JY, Poudel BK, et al. Multilayer-coated liquid crystalline nanoparticles for effective sorafenib delivery to hepatocellular carcinoma. *ACS Appl Mater Interfaces*. 2015;7(20):360–368. doi:10.1021/acsami.5b06203
26. Rand D, Ortiz V, Liu YA, et al. Nanomaterials for X-ray imaging: gold nanoparticle enhancement of X-ray scatter imaging of hepatocellular carcinoma. *Nano Lett*. 2011;11(7):2678–2683. doi:10.1021/nl200858y
27. Kong FY, Zhang JW, Li RF, Wang ZX, Wang WJ, Wang W. Unique roles of gold nanoparticles in drug delivery, targeting and imaging applications. *Molecules*. 2017;22(9):1445. doi:10.3390/molecules22091445
28. Barabadi H, Ovais M, Shinwari ZK, Saravanan M. Anti-cancer green bionanomaterials: present status and future prospects. *Green Chem Lett Rev*. 2017;10(4):285–314. doi:10.1080/17518253.2017.1385856
29. Saifullah B, Buskaran K, Shaikh RB, et al. Graphene oxide–PEG–protocatechuic acid nanocomposite formulation with improved anticancer properties. *Nanomaterials*. 2018;8(10):820. doi:10.3390/nano8100820
30. Bullo S, Buskaran K, Baby R, Dorniani D, Fakurazi S, Hussein MZ. Dual Drugs anticancer nanoformulation using graphene oxide-PEG as nanocarrier for protocatechuic acid and chlorogenic acid. *Pharm Res*. 2019;36(6):91. doi:10.1007/s11095-019-2621-8
31. Barahuie F, Saifullah B, Dorniani D, et al. Graphene oxide as a nanocarrier for controlled release and targeted delivery of an anticancer active agent, chlorogenic acid. *Mater Sci Eng C Mater Biol Appl*. 2017;74:177–185. doi:10.1016/j.msec.2016.11.114
32. Georgakilas V, Tiwari JN, Kemp KC, et al. Noncovalent functionalization of graphene and graphene oxide for energy materials, biosensing, catalytic, and biomedical applications. *Chem Rev*. 2016;116(9):5464–5519. doi:10.1021/acs.chemrev.5b00620
33. Yu L, Wang Z, Mo Z, et al. Synergetic delivery of triptolide and Ce6 with light-activatable liposomes for efficient hepatocellular carcinoma therapy. *Acta Pharm Sin B*. 2021;11(7):2004–2015. doi:10.1016/j.apsb.2021.02.001
34. He M, Yu L, Yang Y, et al. Delivery of triptolide with reduction-sensitive polymer nanoparticles for liver cancer therapy on patient-derived xenografts models. *Chin Chem Lett*. 2020;31(12):3178–3182. doi:10.1016/j.cclet.2020.05.034
35. Yang Y, Liu X, Ma W, et al. Light-activatable liposomes for repetitive on-demand drug release and immunopotentiation in hypoxic tumor therapy. *Biomaterial*. 2021;265:120456. doi:10.1016/j.biomaterials.2020.120456
36. Chen M, Sun Y, Liu H. Cell membrane biomimetic nanomedicines for cancer phototherapy. *Interdis Med*. 2023;1(2):e20220012.
37. Ma W, Chen Q, Xu W, et al. Self-targeting visualizable hyaluronate nanogel for synchronized intracellular release of doxorubicin and cisplatin in combating multidrug-resistant breast cancer. *Nano Res*. 2021;14(3):846–857. doi:10.1007/s12274-020-3124-y
38. Chen G, Yang Y, Xu Q, et al. Self-amplification of tumor oxidative stress with degradable metallic complexes for synergistic cascade tumor therapy. *Nano Lett*. 2020;20(11):8141–8150. doi:10.1021/acs.nanolett.0c03127
39. Yang Y, Yu Y, Chen H, et al. Illuminating platinum transportation while maximizing therapeutic efficacy by gold nanoclusters via simultaneous near-infrared-I/II imaging and glutathione scavenging. *ACS Nano*. 2020;14(10):13536–13547. doi:10.1021/acsnano.0c05541
40. Morales-Cruz M, Delgado Y, Castillo B, et al. Smart Targeting to improve cancer therapeutics. *Drug Des Devel Ther*. 2019;13:3753–3772. doi:10.2147/DDDT.S219489
41. Buskaran K, Bullo S, Hussein MZ, Masarudin MJ, Mohd-Moklas MA, Fakurazi S. Anticancer molecular mechanism of protocatechuic acid loaded on folate coated functionalized graphene oxide nanocomposite delivery system in human hepatocellular carcinoma. *Materials*. 2021;14(4):817. doi:10.3390/ma14040817
42. Steichen SD, Caldorera-Moore M, Peppas NA. A review of current nanoparticle and targeting moieties for the delivery of cancer therapeutics. *Eur J Pharm Sci*. 2013;48(3):416–427. doi:10.1016/j.ejps.2012.12.006

43. Riss TL, Moravec RA, Niles A, et al. Cell viability assays In: Markossian S, Grossman A, Brimacombe K, editors. *Assay Guidance Manual*. Bethesda (MD): Eli Lilly & Company and the National Center for Advancing Translational Sciences. Indianapolis, IN, USA: Bethesda, Eli Lilly & Company; 2004. Available from: https://www.ncbi.nlm.nih.gov/books/NBK53196/. Accessed July 21, 2023.
44. Prieto-Bermejo R, Hernández-Hernández Á. The importance of NADPH oxidases and redox signaling in angiogenesis. *Antioxidants*. 2017;6(2):32. doi:10.3390/antiox6020032
45. Flores-Lopez LZ, Espinoza-Gómez H, Somanathan R. Silver nanoparticles: electron transfer, reactive oxygen species, oxidative stress, beneficial and toxicological effects. *Mini Rev J Appl Toxicol*. 2019;39(1):16–26. doi:10.1002/jat.3654
46. Campbell KJ, Tait SWG. Targeting BCL-2 regulated apoptosis in cancer. *Open Biol*. 2018;8(5):180002. doi:10.1098/rsob.180002
47. Elmore S. Apoptosis: a review of programmed cell death. *Toxicol Pathol*. 2007;35(4):495–516. doi:10.1080/01926230701320337
48. Zamaraev AV, Kopeina GS, Prokhorova EA, Zhivotovsky B, Lavrik IN. Post-translational modification of caspases: the other side of apoptosis regulation. *Trends Cell Biol*. 2017;27(5):322–339. doi:10.1016/j.tcb.2017.01.003
49. Carrington EM, Zhan Y, Brady JL, et al. Anti-apoptotic proteins BCL-2, MCL-1 and A1 summate collectively to maintain survival of immune cell populations both in vitro and in vivo. *Cell Death Differ*. 2017;24(5):878–888. doi:10.1038/cdd.2017.30
50. Plati J, Bucur O, Khosravifar R. Dysregulation of apoptotic signaling in cancer: molecular mechanisms and therapeutic opportunities. *J Cell Biochem*. 2008;104(4):1124–1149. doi:10.1002/jcb.21707
51. Singh R, Letai A, Sarosiek K. Regulation of Apoptosis in health and disease: the balancing act of BCL-2 family proteins. *Nat Rev Mol Cell Biol*. 2019;20(3):175–193. doi:10.1038/s41580-018-0089-8
52. Perini GF, Ribeiro GN, Neto JVP, Campos LT, Hamerschlak N. BCL-2 as therapeutic target for hematological malignancies. *J Hematol Oncol*. 2018;11(1):1–15. doi:10.1186/s13045-018-0608-2
53. Shalini S, Dorstyn L, Dawar S, et al. Old, new and emerging functions of caspases. *Cell Death Differ*. 2015;22(4):526–539. doi:10.1038/cdd.2014.216